Real-time tunable phase response and group delay in broadside coupled split-ring resonators

Xiaoguang Zhao, Jingdi Zhang, Kebin Fan, Guangwu Duan, Jacob Schalch, George R. Keiser, Richard D. Averitt, and X. Zhang

Phys. Rev. B **99**, 245111 — Published 6 June 2019

DOI: 10.1103/PhysRevB.99.245111

Real-time tunable phase response and group delay in broadside coupled split ring resonators

Xiaoguang Zhao[1], Jingdi Zhang[2], Kebin Fan[1], Guangwu Duan[1], Jacob Schalch[2], George R. Keiser[3], Richard D. Averitt[2,*], and X. Zhang[1,*]

[1]*Department of Mechanical Engineering, Boston University, Boston, Massachusetts 02215, USA*

[2]*Department of Physics, University of California, San Diego, La Jolla, California 92093, USA*

[3]*Department of Physics, Washington College, Chestertown, Maryland 21620, USA*

**Corresponding authors: xinz@bu.edu, raveritt@ucsd.edu*

(Received ; revised ; published)

Manipulating the phase of electromagnetic radiation is of importance for applications ranging from communication to imaging. Here, a real-time reconfigurable phase response and group delay of a tunable terahertz metamaterial consisting of dual-layer broadside coupled split ring resonators is demonstrated. Utilizing electrostatic comb-drive actuators, the metamaterial resonant frequency is tuned by changing the lateral distance between the two layers which modifies the transmission amplitude and phase spectrum. The phase modulation is approximately 180˚ in the vicinity of the resonance frequency. In addition, remarkable modulation in the group delay of transmitted pulses (from -7 ps to 3 ps) is evaluated based on the measured frequency response using the convolution method when the lateral distance is changed from 0 to 24 μm. A two-port resonator model, derived from coupled mode theory and supported by finite element full-wave simulations, reveals the underlying physics of the modulation. Specifically, the coupling factor between the two layers plays a critical role, the tuning of which provides a route for structure design and optimization. The capability of tuning the phase response and group delay enables applications, such as phase compensation and group delay equalization at terahertz frequencies.

I. INTRODUCTION

Electromagnetic (EM) metamaterials, comprising sub-wavelength unit-cells, can effectively control the amplitude and phase of EM waves and enable extraordinary effects including negative refraction index, invisibility cloaking and perfect absorption [1-4]. Especially, the ability to engineer the phase response has led to numerous optical applications including wave-front control [5], polarization manipulation [6], and holographic imaging [7], among others. To create functional devices with metamaterials, active tuning schemes via optical [8], thermal [9,10], electrical [11-13], and mechanical [14,15] excitations have been implemented to modulate the EM response. The approaches typically employ a single layer. However, dual-layer metamaterial structures have been proposed to achieve larger tuning and more efficient manipulation of the EM properties due to near field coupling between two layers [16-23]. This includes, as examples, tuning of the effective permittivity and permeability, and chirality. In these dual layer MMs, such as broadside coupled split ring resonators (BC-SRRs), the effects of coupling on mode splitting have been investigated using Lagrangian approaches to predict the resonant frequencies [16-19] and numerical approaches have been used to study the scattering parameters under varied coupling conditions [22-23]. To understand the role of coupling and ease the design of optimized coupled resonators, it is desirable to have a concise and accurate lumped-parameter model that fully predicts the modulation of the amplitude and phase of the incoming electromagnetic wave.

Recently, we demonstrated a dual-layer terahertz metamaterial in which the resonant response was controlled in real time by micromachined comb-drive actuators [24]. Although the mechanism of the frequency tuning and amplitude modulation was discussed using a qualitative description and quantitative numerical simulations, the phase modulation was not explicitly explored and an accurate lumped-parameter model was not implemented.

In this paper, we present tunable phase modulation, initiated by driving the micromachined actuators that control the lateral distance between the BC-SRRs. The phase shift and group delay near the resonant frequencies are explored. We show that a sudden jump in the phase shift and group delay occurs at a critical distance, associated with a critical coupling strength. In order to investigate the crucial role of coupling in determining the property of BC-SRRs, we propose a lump-parameter model within the framework of the coupled mode theory (CMT). The CMT model predicts the transmission response of the BC-SRRs with different relative lateral distances and captures the essence of phase and group delay modulation. We can optimize the tunable phase and

group delay of the BC-SRRs with the guidance of the CMT model to construct functional THz devices, such as phase modulators. The proposed CMT model can serve as a general tool for understanding other coupled metamaterial structures.

II. EXPERIMENTS OF THE TUNABLE PHASE RESPONSE AND GROUP DELAY

The real-time tunable metamaterial is composed of dual-layer split ring resonators in the broadside coupled configuration, as shown in Fig. 1 (a). One layer is fixed on a silicon nitride (SiN_x) thin film, with the second layer mounted on a 10-μm-thick silicon (Si) plate connected to comb-drive actuators. The two layers are bonded together with an out-of-plane distance of ~20 μm to promote strong electric and magnetic coupling between the layers. The periodicity of SRR in each array is 58 μm and the dimension of the individual SRRs is 40 μm by 40 μm with a line width of 11 μm. The gap-size of the SRRs for each layer is slightly different to compensate the resonant frequencies between the two layers due to the different substrate materials. The gap-sizes are 2 μm and 16 μm for the SRRs on the stationary SiNx thin film and movable SRRs on Si plate, respectively. The coupling strength between the two layers is dependent on the lateral relative position [18,22]. A DC-voltage driven comb-drive actuator translates the movable layer to adjust the relative lateral position of the two SRRs layers, and hence the coupling strength of the neighboring layers.

The tunable metamaterial structure is fabricated using bulk micromachining [24], and the microscope images of the BC-SRRs under varied voltages are shown in Fig. 1 (b). We can adjust their relative lateral distance (Δ) from 0 μm through 24 μm continuously using an applied voltage to shift the movable SRRs (Fig. 1(b)). The transmission spectra of the BC-SRRs for various Δ are characterized using THz time domain spectroscopy (TDS) with 2 V increments of the applied voltage (spanning 110 V). Figs. 1(c) and (d) are the amplitude and phase of the transmission spectrum at different lateral positions. In order to accurately analyze the phase response and calculate the group delay, we unwrap the measured phase to avoid artificial singularities that would otherwise arise in the group delay response. When the two SRR arrays are aligned, i.e. $\Delta = 0$ μm, there are two well-separated resonance modes at 1.03 THz and 1.23 THz. In the phase spectrum, the phase of transmission exhibits ~90° variation for both 1.03 THz mode (-81° to -10°) and 1.23 THz mode (-38° to 58°). With the increasing lateral distance, the first resonance mode blue-shifts and the second mode red-shifts, simultaneously. The transmission amplitude of the first mode decreases along with the resonance blue-shift, which is indicative of a stronger resonance. As a

result, the phase variation around the first resonant frequency further increases. It is approximately 140° for Δ = 12 μm. For a lateral distance of 15 μm, the resonant frequencies merge towards each other. Interestingly, the phase variation around the first resonant frequency is ~ -180° (from -154° to -320°), instead of a positive value for the smaller Δ values. The negative phase variation starts to prevail for lateral distances over 15 μm. The phase modulation is approximately 180° at 1.06 THz.

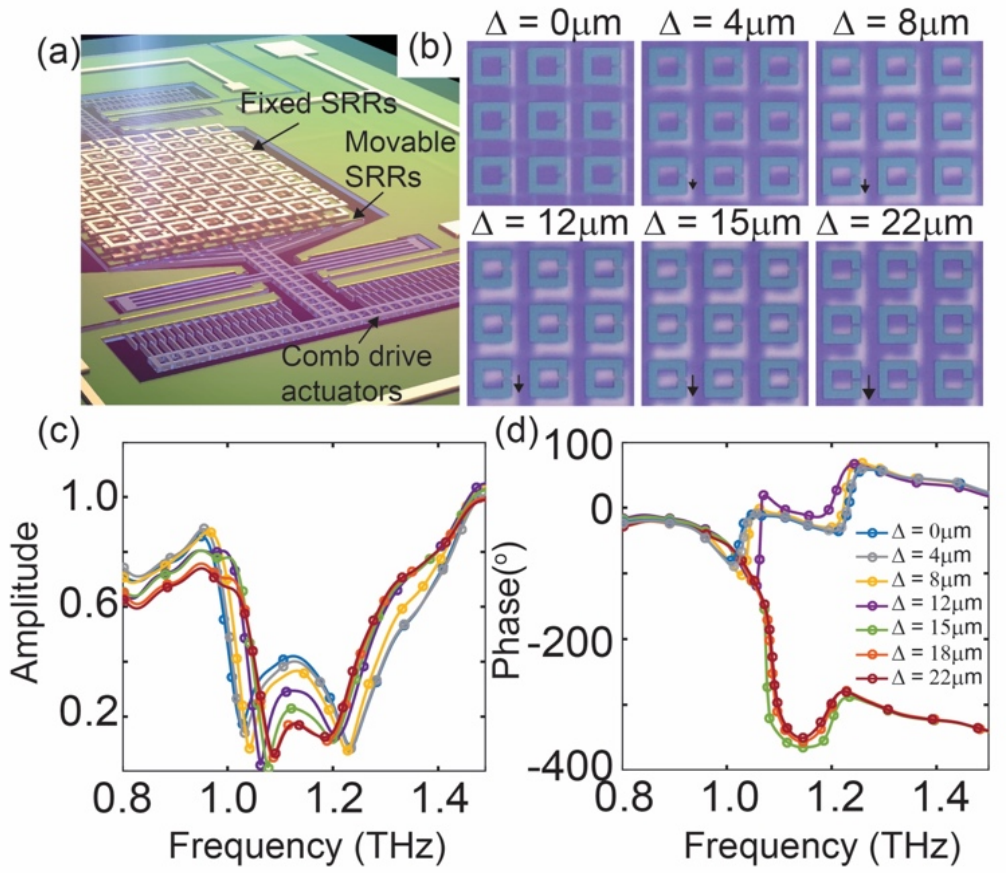

FIG. 1. (a) Illustration of real-time tunable metamaterial based on broadside coupled split ring resonator (BC-SRRs). It is comprised of a fixed array of split ring resonators (top layer) and a movable array driven by comb-drive actuators. (b) The microscope image of the bi-layer SRRs for various relative lateral distances (Δ). The dark SRR is fixed, the bright one is movable. (c) and (d) show the amplitude and phase spectra of the BC-SRRs for different Δ, measured using THz time domain spectroscopy.

The experimental phase shift (PS) diagram of the BC-SRRs as a function of lateral distance and frequency (Fig. 2(a)) indicates the existence of a critical lateral distance of 15 μm, where a sudden jump of the phase variation occurs. The group delay, $\tau_G = -d\varphi/d\omega$, can be calculated from the PS diagram. Figs. 2(b) and 2(c) show the tunability of the group delay by varying lateral Δ. At zero

lateral distance, the negative group delay (NGD) resides in the vicinity of the resonant frequencies, e.g. τ_G = -10.22 ps at 1.03 THz and τ_G = -11.86 ps at 1.23 THz. The NGD originates from the strong anomalous dispersion of the Lorentzian–like medium [25,26], which is the BC-SRR metamaterial in our case. The bandwidths for the negative group delay are 50 GHz and 64 GHz for the lower and higher resonant frequencies, respectively. An example of the NGD in the time-domain is illustrated by calculating the time domain response for a narrow band incident pulse, with a center frequency of 1.03 THz and 40 GHz bandwidth, as shown in Fig. 1(d). Its interaction with the BC-SRRs is calculated using convolution, as detailed in the Appendix A. The envelope peak arrives approximately 7 ps earlier than the incident wave, indicating a negative group delay, when the SRRs are aligned (Δ = 0 μm). When the lateral distance approaches 22 μm, the group delay turns to be a positive value (~ 3 ps). The group delay describes the time delay of the amplitude envelope of the incident wave. The effect of the metamaterial on delaying the envelope of the incident wave depends on the central frequency of the incident wave and the pulse bandwidth. We define the fractional delay (FD = τ_G/τ_P, where τ_P is the pulse duration) to describe efficiency of the metamaterial in shifting of the waveforms. The FD is approximate -0.04 and 0.02 for Δ = 0 μm and 22 μm, respectively. A more detailed discussion can be found in Appendix A and Table A1. Visualization 1 in the Supplemental Material [27] demonstrates real-time tuning group delay by actuating the MEMS actuators. The phenomenon of negative and tunable group delay demonstrated here may be potentially exploited in designing an adaptive THz group delay equalizer, which can compensate the positive group delay in waveguides or other THz components with similar operating mechanisms to that at microwave frequencies [28,29]. The group delay at one specific frequency is tuned in a continuous fashion, which could, in principle, be observed with fine enough actuation of the comb-drive. The group delay at the resonant frequency varies rapidly near the critical lateral distance. Further, the transmission amplitude is nearly zero at this condition. The combination of the transmission amplitude and group delay response enables the continuous modulation of the metamaterial response. A similar transition of the group delay from negative to positive values (driven by micro-cantilevers) has been reported for the in-plane coupled resonator [30].

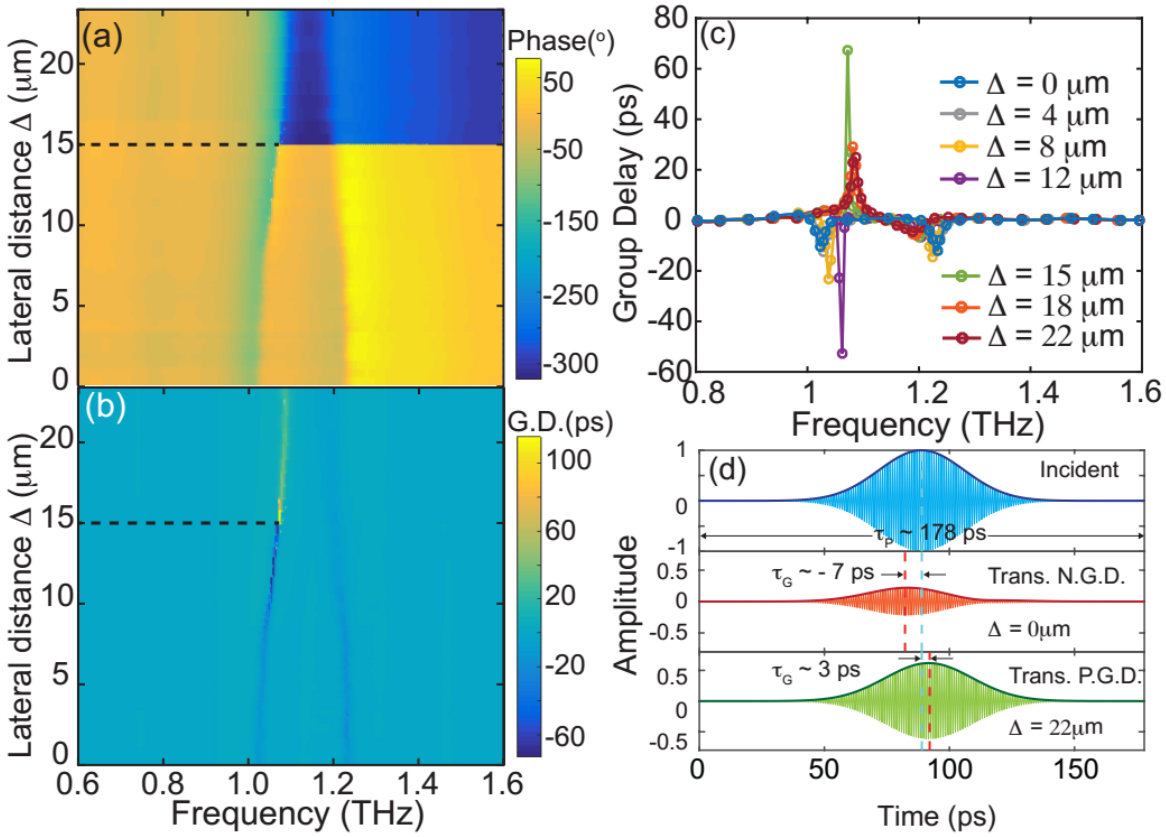

FIG. 2. (a)The measured PS diagram of the BC-SRRs by sweeping Δ. A sudden jump in the phase is observed when Δ ~ 15 μm. (b) The calculated group delay for different Δ. (c) Group delay for some specific lateral distances. Negative group delay is achieved in vicinity of the resonant frequency for a small Δ. For Δ exceeding 15 μm, the group delay is positive for the first mode. (d) The calculated time domain response of the reconfigurable BC-SRRs to incident waves with center frequency of 1.03 THz and 10 GHz bandwidth. The group delay is approximately -7 ps for Δ = 0 μm and ~ 3 ps for Δ = 22 μm. G. D.: Group delay. N.G.D.: Negative group delay. P.G.D.: Positive group delay.

III. COUPLED MODE THEORY MODEL OF THE BC-SRRS

The modulation of the resonant frequencies, the phase response, and the group delay originates from changing the coupling strength between the SRRs of the two layers with Δ. Different approaches, including the equivalent circuit model [31] and Lagrangian method [16,18], have been employed to describe the resonant response of metamaterials. We utilize coupled mode theory (CMT) to understand the experimental results. To simplify mathematical derivation, we consider BC-SRRs comprising identical SRRs for the top and bottom layers comprising the BC-SRR metamaterial, noting that this deviates from experiment. Finite element simulations using CST Microwave Studio

are employed to validate the CMT model. To start with, consider a single layer SRR whose transmission response can be modeled as [12,32,33]

$$t = \frac{j(\omega - \omega_0) + 1/\tau_0}{j(\omega - \omega_0) + (1/\tau_0 + 1/\tau_e)} \quad (1)$$

where ω_0 is the resonant angular frequency, and $1/\tau_0$ and $1/\tau_e$ denote the decay rate due to the intrinsic loss (absorption) and radiation loss, respectively. We define two dimensionless parameters $Q_0 = \omega_0\tau_0/2$ and $Q_e = \omega_0\tau_e/2$, representing the intrinsic and radiative quality factors [34]. For the aforementioned single-layer SRRs on the SiN_x thin film, we estimate the quality factors by treating the SRR as an electrically small loop antenna. The radiative quality factor can be evaluated as $Q_e = [6 \ln(2P/w)]/[\pi(\beta_0 P)2]$, in which P is the periodicity of the SRR, w is the width of the wire, and β_0 is the wavenumber at the resonant frequency in free-space [35]. The intrinsic quality factor can be calculated by $Q_0 = (\omega_0 L)/R$, where L is the inductance of the square loop and R is the resistance. The dimensions of our structure yield quality factors $Q_e \approx 6.5$ and $Q_0 \approx 61$. The calculated transmission response based on CMT agrees well with the simulation results using finite element method (FEM) shown in Fig. 3(a), validating the CMT model for single layer SRRs. In vicinity of the resonant frequency, the transmission amplitude approaches the minimum value and the phase varies from -55° to 55°, meaning that the group delays are negative in this band (shaded region in Fig. 3(a)). The transmission response can be represented in Smith curves, which are trace of transmission coefficient on a complex plane as frequency increases from 0 to ∞ [12], as shown in Fig. 3(b). In the Smith chart, the x and y axes correspond to the real and imaginary parts of the transmission coefficient, enabling consideration of both the amplitude and phase of the SRRs directly from the Smith curve. For a single SRR, the transmission response is bounded within the right part of the Smith chart for different combinations of the quality factors (Q_0 and Q_e). The resonance corresponds to the minimum distance to the origin. For the single SRRs, the resonance frequencies are the crossing points on the x-axis (as shown by the dots in the Smith curve). As such, the phase response is bounded between -90^0 and 90^0. The Smith curve approaches the origin as Q_0 approaches to infinity. However, it is impossible to reach the origin and the left part of the Smith chart.

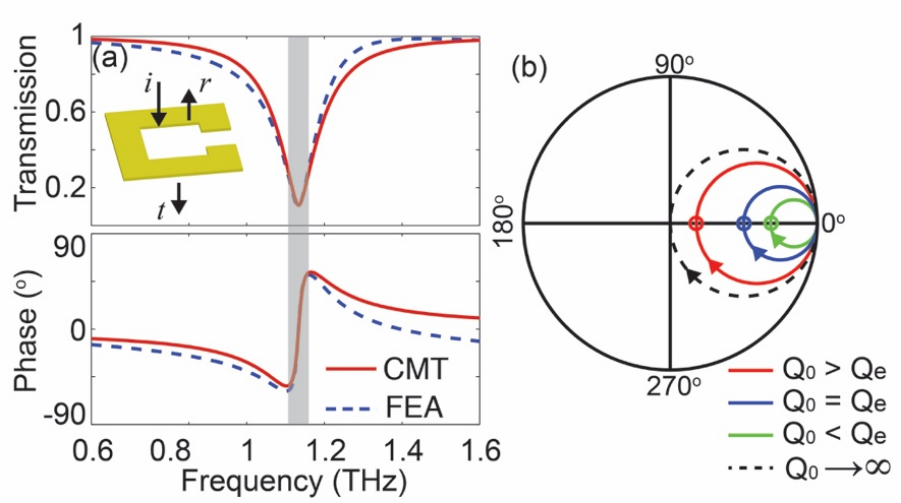

FIG. 3. (a) The theoretical transmission response (solid line) of the single SRR based on coupled mode theory (CMT) and its corresponding simulation result (dash line) using finite element analysis (FEA). Inset shows the schematic of a single SRR, in which i, r and t stand for incidence, reflection and transmission, respectively. (b) The calculated Smith curves based on CMT for different combinations of quality factors. Colored circle points corresponding to the real-axis crossing points (Pr).

According to CMT, the coupling between two resonators can lead to mode splitting, i.e. creating two resonant modes - a symmetric mode and an anti-symmetric mode [36]. Within the framework of CMT, the transmission response of BC-SRRs including two identical SRRs can be described by

$$t = 1 - \frac{\frac{1}{\tau_e}(1+\cos(\phi))}{j(\omega-\omega_s)+\frac{1}{\tau_e}(1+\cos(\phi))+\frac{1}{\tau_0}} - \frac{\frac{1}{\tau_e}(1-\cos(\phi))}{j(\omega-\omega_a)+\frac{1}{\tau_e}(1-\cos(\phi))+\frac{1}{\tau_0}} \tag{2}$$

where ω_s and ω_a are the resonant angular frequencies of the symmetric mode and anti-symmetric mode, respectively, and $\phi = \pi+\beta l$ is the phase difference between the two resonators, in which β is the wave number in free space and l is the vertical distance between the SRRs. A detailed derivation of the model can be found in the Supplemental Material [27]. Based on the coupling between the two SRRs, the resonant frequencies can be estimated by

$$\omega_s = \omega_0 - (\mu\omega_0 - \frac{1}{\tau_e}\sin(\phi)), \omega_a = \omega_0 + (\mu\omega_0 - \frac{1}{\tau_e}\sin(\phi)) \tag{3}$$

in which μ is the direct coupling factor between the resonators, and $1/\tau_e \sin(\phi)$ means the indirectly coupling through wave propagation [36]. The coupling factor (μ) represents the total coupling strength, determined by inductive and capacitive coupling factors that can be calculated using a Lagrangian approach [18,19,37]. In the finite element model, we build two identical SRRs on SiNx thin films separated by a 20-μm-thick air spacer (i.e. l = 20 μm) and apply periodic boundary conditions. The frequency spectra at different relative lateral distances (Δ) between SRRs are given by the frequency solver in CST Microwave Studio. As shown in Fig. 4 (a), we can match the finite element analysis (FEA) results for Δ in the range from 0 to 23 μm by sweeping μ from 0.13 to 0.06 using the CMT model, verifying that Eq. (2) can accurately capture the EM response of the BC-SRRs. The increased relative lateral distance decreases the coupling strength, merging the two resonant modes according to Eq. (3). The modulated transmission amplitude given by CMT with the decreased coupling factor qualitatively coincides with the measured spectra (Fig. 1(c)). The two resonant modes combine to one mode at a critical coupling factor (μ_c ~0.07 for our case). The experimental results slightly deviate from the CMT model since the two SRR arrays in the experimental device are not identical.

It is important to note that the coupling factor dependence of the phase response (Fig. 4(b)) is similar to the experimental results in Fig. 1 (d). When the coupling is strong (μ = 0.13), ~ 90$^{\mathbf{o}}$ phase variation shows up at both the symmetric and anti-symmetric modes. When the coupling weakens, the phase variation at the symmetric mode becomes more pronounced due to the increase of the resonance magnitude. At critical coupling, the phase variation at the resonant frequency transits from a positive to negative and stays negative for further decrease of the coupling. Tuning the coupling factor can consequently modulate the group delay as shown in Fig. 4 (c), in agreement with the experiment (Fig. 2(c)). For strong coupling, a negative group delay is achieved at the resonant frequencies. When the coupling factor is below the critical value, the resonance group delay is positive and decreases along with the decreasing coupling factor. A large group delay is achieved when the coupling factor is in the vicinity of the critical coupling.

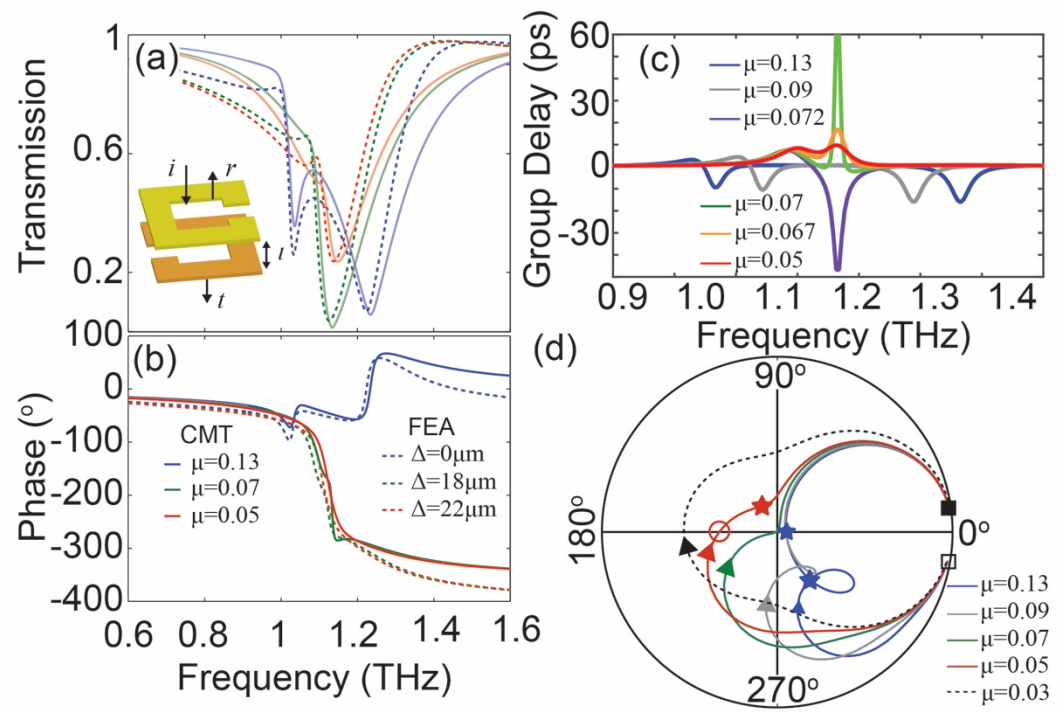

FIG. 4. The amplitude (a) and phase (b) of the complex transmission coefficients of the BC-SRRs based on the CMT model (Solid lines) and FEA simulation (dash lines). The theoretical group delay (c) and Smith curves (d) for different coupling factors calculated using the CMT model.

The transmission Smith curves of the BS-SRRs with different coupling factors are shown in Fig. 4(d), which facilitates determining the critical coupling strength. In the Smith curve, as the frequency increases, the transmission coefficient varies from the hollow square to solid one following the traces as shown in Fig. 4(d). The Smith curve for strong coupling, as shown by the blue curve, lies in the right-hand part of the chart with two points (as indicated by blue stars) that are with minimum distances to the origin, corresponding to the two resonant modes. The phase tends to span from -90° to 90° since it crosses the x-axis in the left-hand half of the complex plane. With a decreasing coupling strength, the bottom part (associated with the symmetric mode) is moving to the fourth quadrant gradually to extend the phase coverage. When the coupling factor decreases to the critical value, the Smith curve crosses the origin (as shown by the green curve), meaning that the BC-SRRs has a single resonant frequency and zero-transmission. We can evaluate the critical coupling using

$$\mu_c = \sqrt{\left(\frac{\sin\phi}{2Q_e}\right)^2 - \left(\frac{1}{2Q_0}\right)^2} + \frac{\sin\phi}{2Q_e} \tag{4}$$

which yields $\mu_c \approx 0.07$ in Fig. 4(d). The critical coupling factor is associated with the quality factors (Q_e and Q_0) of the single resonator and their phase difference (ϕ). Eq. 4 provides some guidance for BC-SRRs device design and optimization. For example, we can increase the critical coupling factor by decreasing Q_e and increasing Q_0 via modifying the structure of the resonators. Therefore, the required tuning range of the coupling factor to change the sign of group delay from negative to positive is decreased. Notably, when the coupling factor is smaller than μ_c, taking the red curve in Fig. 4(d) as one example, the Smith curve extends to four quadrants to cover the 0-360° phase range in the spectrum. At the same time, the Smith curve crosses the x-axis in the right half-plane (as indicated by the red circle), meaning a negative phase shift and positive group delay near the resonance frequency. When $\mu = 1/(2Q_e)\cdot\sin(\phi) \approx 0.035$, ω_s and ω_a become degenerated (i.e. $\omega_s = \omega_a = \omega_0$), meaning that the effects of direct and indirect coupling are completely cancelled by each other. In this condition, the pear-like Smith curve (dashed line in Fig. 4 (d)), which is symmetric with respect to the real axis, is achieved. The minimum transmission is located at the intersection of the Smith curve and the imaginary axis. With the help of Eq. (2) and the Smith chart derived from it, we can predict the impact of the coupling and quality factors to guide the design of the BC-SRRs, as shown in Fig. S2 in the Supplemental Material [27]. Since the structural details are not required for CMT modelling, this approach can be applied to other metamaterial designs, as demonstrated in the Supplemental Material [27,38].

IV. CONCLUSION

In conclusion, we have demonstrated a real-time tunable metamaterial based on BC-SRRs and MEMS actuators. The amplitude and phase of the transmission can be modulated through actuating the relative lateral distance of the two SRR layers with the resultant group delay tuned from -7 ps to 3 ps at 1.03 THz in experiments. A sudden jump in the phase and group delay response occurs at a critical lateral distance. To understand the response of the BC-SRRs, we have developed a lumped-parameter model based on CMT. The agreement among the analytical CMT model, the FEM simulation and experiment results validates the theoretical model, and unveils the effect of coupling factor on the response of BC-SRRs. A critical coupling, at which strength sharp phase and group delay variations occurred, is identified. Furthermore, the CMT model and Smith curves

predict the response of metamaterial composed of coupled resonators and provide us guidelines for the future structure design and optimization of functional metamaterial devices.

ACKNOWLEDGEMENTS

The authors would like to acknowledge the support from National Science Foundation (NSF) (ECCS-1309835 and ECCS-1810252) and DOE—Basic Energy Sciences (DE-FG02-09ER46643). We thank Boston University Photonics Center for technical support. X. Zhao and J. Zhang contributed equally to this work.

APPENDIX A: CALCULATION OF THE NARROW BAND RESPONSE

The real time tunable BC-SRR metamaterial device was characterized using terahertz time domain spectroscopy (THz-TDS), which is a broadband method. In order to demonstrate negative and tunable group delay in the dual-layer metamaterials, we used the experimental transmission spectrum to calculate the narrow band response using convolution methods, detailed as follows. We used a simulated narrow band incident pulse [$i(t)$] with a center frequency of 1.03 THz and bandwidth of 40 GHz. Fourier transforming the incident pulse provides the frequency domain response [$i(\omega)$], as show in Fig. A1(a). The spectrum of the transmitted wave [Fig. A1(c)] was calculated by multiplying $i(\omega)$ with the experimentally determined transmission spectrum of the device [$t(\omega)$, as shown in Fig. A1(b)]. Finally, the inverse Fourier transform was performed to obtain the transmission in the time domain [Fig. A1(d)]. A video demonstrating the real-time tunable group delay can be found in Supplemental Material [27].

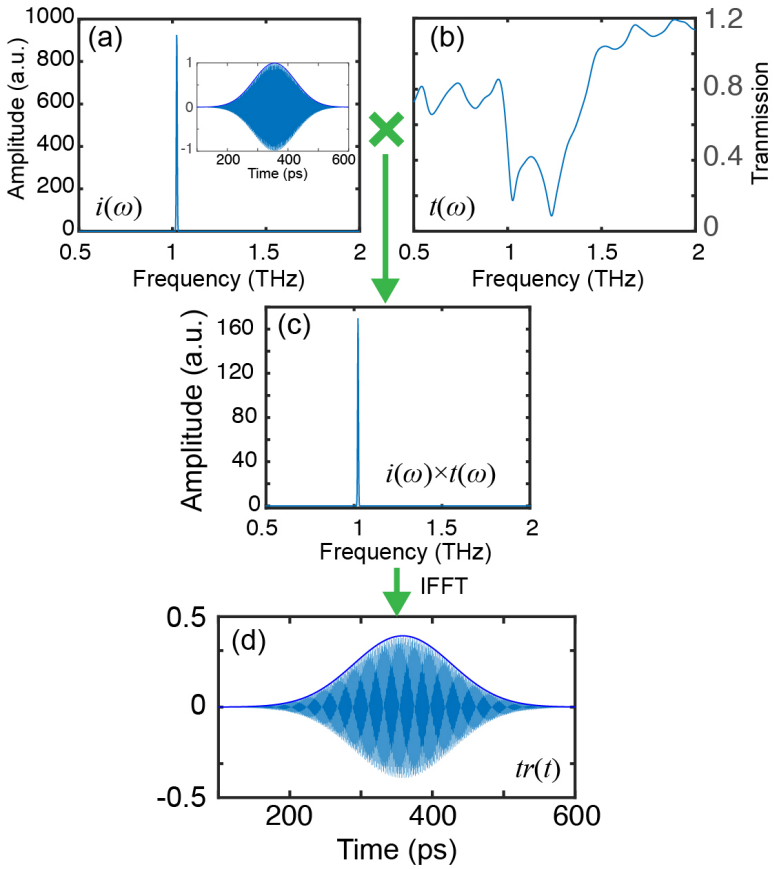

FIG. A1. Procedure to calculate the time domain response for a narrow band pulse. (a) Spectrum of the incident wave (inset: temporal signal of the incidence). (b) Transmission spectrum of the dual-layer metamaterial. (c) Product of i(ω) and t(ω), i.e. the amplitude spectrum of the transmitted wave. (d) Time domain transmission wave calculated by inverse Fourier transform of spectrum (c).

We defined a fractional delay FD = τ_G /τ_P (where τ_G is the group delay and τ_P is the pulse duration), to describe the effect of the metamaterial on the THz waves. A larger absolute value of the FD means that the metamaterial has a greater impact on delaying (+)/advancing (-) the waveform. The group delay and FD of the BC-SRRs for the narrow band pulse are related to the bandwidth of the incident wave. As shown in Table S1, negative group delays are obtained for the bandwidth increasing from 10 to 50 GHz when the SRRs are aligned (Δ = 0 μm). With the increased bandwidth, the absolute value of the group delay decreases from 10.1 ps to 6.1 ps due to the finite bandwidth of the metamaterials device. However, the FD decreases from -0.02 to -0.04, indicating an increased group delay, because of the shortened the pulse duration (smaller τ_P) for larger bandwidth. When Δ = 22 μm, the increased bandwidth leads to increased FD as well. Table

A1 reveals that the tunable group delay depends on the bandwidth of the incident pulse. The narrower band incidence exhibits larger group delay while broader band incidence shows larger FD.

Table A1. The group delay and FD of the tunable metamaterial with different bandwidth at the center frequency of 1.03 THz.

Central Frequency of pulse (THz)	Pulse Bandwidth (GHz)	Lateral shift (Δ, μm)	Group delay (τ_G, ps)	FD
1.03	10	0	-10.1	-0.020
		22	2.8	0.006
1.03	20	0	-9	-0.025
		22	5	0.015
1.03	30	0	-6.7	-0.028
		22	3.1	0.013
1.03	40	0	-6.7	-0.038
		22	3.2	0.018
1.03	50	0	-6.1	-0.041
		22	2.9	0.020

References:

[1] R. A. Shelby, D. R. Smith, S. Schultz, Science **292**, 77 (2001).

[2] S. Zhang, W. Fan, N. C. Panoiu, K. J. Malloy, R. M. Osgood, S. R. J. Brueck, *Phys. Rev. Lett*. **95**, 137404 (2005).

[3] D. Schurig, J. J. Mock, B. J. Justice, S. A. Cummer, J. B. Pendry, A. F. Starr, D. R. Smith, *Science* **314**, 977 (2006).

[4] N. I. Landy, S. Sajuyigbe, J. J. Mock, D. R. Smith, W. J. Padilla, *Phys. Rev. Lett.* **100**, 207402 (2008).

[5] N. Yu, P. Genevet, M. A. Kats, F. Aieta, J.-P. Tetienne, F. Capasso, Z. Gaburro, *Science* **334**, 333 (2011).

[6] N. K. Grady, J. E. Heyes, D. R. Chowdhury, Y. Zeng, M. T. Reiten, A. K. Azad, A. J. Taylor, D. A. R. Dalvit, H.-T. Chen, *Science* **340**, 1304 (2013).

[7] S. Larouche, Y.-J. Tsai, T. Tyler, N. M. Jokerst, D. R. Smith, *Nat. Materials* **11**, 450 (2012).

[8] H.-T. Chen, J. F. O'Hara, A. K. Azad, A. J. Taylor, R. D. Averitt, D. B. Shrekenhamer, W. J. Padilla, *Nat. Photonics* **2**, 295 (2008).

[9] W. Lewandowski, M. Fruhnert, J. Mieczkowski, C. Rockstuhl, E. Gorecka, *Nat. Commun.* **6**, 6590 (2015).

[10] H. Tao, A. C. Strikwerda, K. Fan, W. J. Padilla, X. Zhang, R. D. Averitt, *Phys. Rev. Lett.* **103**, 147401 (2009).

[11] H.-T. Chen, W. J. Padilla, J. M. O. Zide, A. C. Gossard, A. J. Taylor, R. D. Averitt, *Nature* **444**, 597 (2006).

[12] Z. Miao, Q. Wu, X. Li, Q. He, K. Ding, Z. An, Y. Zhang, L. Zhou, *Phys. Rev. X* **5**, 041027 (2015).

[13] K. Fan, J. Suen, X. Wu, W. J. Padilla, *Opt. Express* **24**, 25189 (2016).

[14] W. M. Zhu, A. Q. Liu, T. Bourounia, D. P. Tsai, J. H. Teng, X. H. Zhang, G. Q. Lo, D. L. Kwong, *Nat. Commun.* **3**, 1274 (2011).

[15] X. Zhao, J. Schalch, J. Zhang, H. R. Seren, G. Duan, R. D. Averitt, X. Zhang, *Optica* **5**, 303 (2018).

[16] N. Liu, H. Liu, S. Zhu, H. Giessen, *Nat. Photonics* **3**, 157 (2009).

[17] T. Q. Li, H. Liu, T. Li, S. M. Wang, J. X. Cao, Z. H. Zhu, Z. G. Dong, S. N. Zhu, X. Zhang, *Phys. Rev. B* **80**, 115113 (2009).

[18] D. A. Powell, M. Lapine, M. V. Gorkunov, I. V. Shadrivov, Y. S. Kivshar, *Phys. Rev. B* **82**, 155128 (2010).

[19] H. Liu, J. X. Cao, S. N. Zhu, N. Liu, R. Ameling, H. Giessen, *Phys. Rev. B* **81**, 241403 (2010).

[20] E. Plum, J. Zhou, J. Dong, V. A. Fedotov, T. Koschny, C. M. Soukoulis, N. I. Zheludev, *Phys. Rev. B* **79**, 035407 (2009).

[21] X. Xiong, W.-H. Sun, Y.-J. Bao, M. Wang, R.-W. Peng, C. Sun, X. Lu, J. Shao, Z.-F. Li, N.-B. Ming, *Phys. Rev. B* **81**, 075119 (2010).

[22] E. Ekmekci, A. C. Strikwerda, K. Fan, G. Keiser, X. Zhang, G. Turhan-Sayan, R. D. Averitt, *Phys. Rev. B* **83**, 193103 (2011).

[23] G. R. Keiser, A. C. Strikwerda, K. Fan, V. Young, X. Zhang, R. D. Averitt, *Phys. Rev. B* **88**, 024101 (2013).

[24] X. Zhao, K. Fan, J. Zhang, G. R. Keiser, G. Duan, R. D. Averitt, X. Zhang, *Microsyst. & Nanoeng.* **2**, 16025 (2016).

[25] G. Dolling, C. Enkrich, M. Wegener, C. M. Soukoulis, S. Linden, *Science* **312**, 892 (2006).

[26] M. Kandic, G. E. Bridges, *Prog. Electromagn. Res.* **134**, 227 (2013).

[27] See Supplemental Material for evaluation of the tunable group delay, derivation of the coupled mode theory model for the coupled resonators, details of the analysis, and visualization of the tunable response.

[28] S. Lucyszyn, I. D. Robertson, A. H. Aghvami, *Electron. Lett*. **29**, 798 (1993).

[29] D. Solli, R. Y. Chiao, J. M. Hickmann, *Phys. Rev. E* **66**, 056601 (2002).

[30] P. Pitchappa, M. Manjappa, C. P. Ho, Y. Qian, R. Singh, N. Singh, C. Lee, *Appl. Phys. Lett*. **108**, 111102 (2016).

[31] K. Azad, A. J. Taylor, E. Smirnova, J. F. O'Hara, *Appl. Phys. Lett.* **92**, 011119 (2008).

[32] H. A. Haus, *Waves and Fields in Optoelectronics*, (Prentice-Hall, New Jersey, 1984).

[33] S. Fan, W. Suh, and J. D. Joannopoulos, *J. Opt. Soc. Am. A* **20**, 569 (2003).

[34] C. Manolatou, M. J. Khan, S. Fan, P. R. Villeneuve, H. A. Haus, J. D. Joannopoulos, *IEEE J. Quantum Electron.* **35**, 1322-1331 (1999).

[35] G. A. Mavridis, D. E. Anagnostou, M. T. Chryssomallis, *IEEE Trans. Antennas Propag*. **53**, 216-224 (2011).

[36] Q. Li, T. Wang, Y. Su, M. Yan, M. Qiu, *Opt. Express*, **8**, 8367 (2010).

[37] B. Kante, Y.-S. Park, K. O'Brien, D. Shuldman, N. D. Lanzillotti-Kimura, Z. J. Wong, X. Yin, X. Zhang, *Nat. Communications* **3**, 1180 (2012).

[38] T. Q. Li, H. Liu, T. Li, S. M. Wang, J. X. Cao, Z. H. Zhu, Z. G. Dong, S. N. Zhu, X. Zhang, *Phys. Rev. B* **80**, 115113 (2009).